
Triple descent and the two kinds of overfitting: Where & why do they appear?

Stéphane d’Ascoli

Department of Physics
École Normale Supérieure
Paris, France
stephane.dascoli@ens.fr

Levent Sagun

Facebook AI Research
Paris, France
leventsagun@fb.com

Giulio Biroli

Department of Physics
École Normale Supérieure
Paris, France
giulio.biroli@ens.fr

Abstract

A recent line of research has highlighted the existence of a “double descent” phenomenon in deep learning, whereby increasing the number of training examples N causes the generalization error of neural networks to peak when N is of the same order as the number of parameters P . In earlier works, a similar phenomenon was shown to exist in simpler models such as linear regression, where the peak instead occurs when N is equal to the input dimension D . In both cases, the location of the peak coincides with the interpolation threshold. In this paper, we show that despite their apparent similarity, these two scenarios are inherently different. In fact, both peaks can co-exist when neural networks are applied to noisy regression tasks. The relative size of the peaks is governed by the degree of nonlinearity of the activation function. Building on recent developments in the analysis of random feature models, we provide a theoretical ground for this sample-wise *triple descent*. As shown previously, the *nonlinear peak* at $N = P$ is a true divergence caused by the extreme sensitivity of the output function to both the noise corrupting the labels and the initialization of the random features (or the weights in neural networks). This peak survives in the absence of noise, but can be suppressed by regularization. In contrast, the *linear peak* at $N = D$ is solely due to overfitting the noise in the labels, and forms earlier during training. We show that this peak is implicitly regularized by the nonlinearity, which is why it only becomes salient at high noise and is weakly affected by explicit regularization. Throughout the paper, we compare the analytical results obtained in the random feature model with the outcomes of numerical experiments involving realistic neural networks.

Introduction

A few years ago, deep neural networks achieved breakthroughs in a variety of contexts [1, 2, 3, 4]. However, their remarkable generalization abilities have puzzled rigorous understanding [5, 6, 7]: classical learning theory predicts that generalization error should follow a U-shaped curve as the number of parameters P increases, and a monotonous decrease as the number of training examples N increases. Instead, recent developments show that deep neural networks, as well as other machine learning models, exhibit a starkly different behaviour [8, 9, 10, 11, 12]. In the absence of regularization, increasing P and N respectively yields parameter-wise and sample-wise *double descent* curves, whereby the generalization error first decreases, then peaks at the *interpolation threshold* (at which point training error vanishes), then decreases monotonically again. This peak¹

¹Also called the *jamming* peak due to similarities with a well-studied phenomenon in the Statistical Physics literature [13, 14, 15, 16, 17].

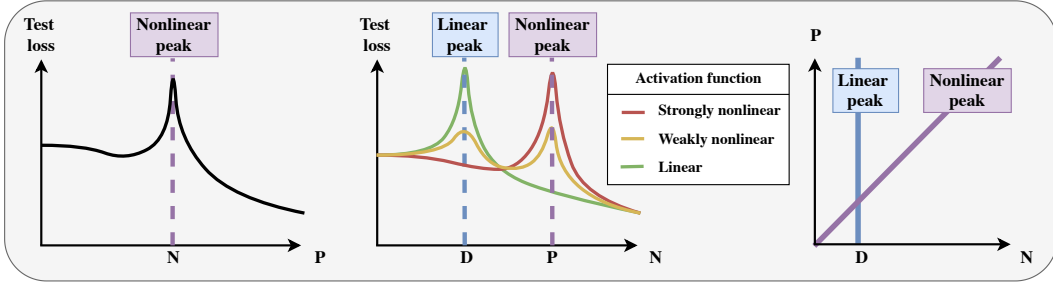


Figure 1: **Left:** The parameter-wise profile of the test loss exhibits double descent. **Middle:** The sample-wise profile can, at high noise, exhibit double or triple descent² depending in particular on the degree of nonlinearity. **Right:** Color-coded location of the peaks in the (P, N) phase space.

was shown to be related to a sharp increase in the variance of the estimator [17, 10], and can be suppressed by regularizing or ensembling procedures [10, 18, 19].

Although double descent has recently gained much interest in the context of deep learning, a seemingly similar phenomenon has been well-known for several decades for simpler models such as linear regression [13, 14, 20, 21]. However, in the context of linear models, the number of parameters P is not a free parameter and is necessarily equal to the input dimension D . The interpolation threshold occurs at $N = D$, and coincides with a peak in the test loss which we refer to as the *linear peak*. For neural networks with nonlinear activations, the interpolation threshold is instead observed when the number of training examples is of the same order as the total number of training parameters, i.e. $N \sim P$: we refer to the corresponding peak as the *nonlinear peak*. Somewhere in between these two scenarios lies the case of neural networks with *linear* activations. They have $P > D$ parameters, but only D of them are independent: the interpolation threshold occurs at $N = D$. However, their dynamical behaviour shares some similarities with that of deep nonlinear networks, and their analytical tractability has given them significant attention [22, 23, 6].

In this work, we unveil the similarities and the differences between these two peaks. In particular, we address the following questions:

- Are the linear and nonlinear peaks two different phenomena, and if so, can we differentiate their sources?
- How does the activation function affect these peaks?
- Can they both be suppressed by regularizing or ensembling? Under a given dynamics, do they appear at the same time during training?

Contribution In modern neural networks, the double descent phenomenon is mostly studied by increasing the number of parameters P (Fig. 1, left), and more rarely, by increasing the number of training examples N (Fig. 1, middle). The analysis of linear models is instead performed by varying the ratio P/N . By studying the full (P, N) phase space (Fig. 1, right), we disentangle the role of the linear and the nonlinear peaks in modern neural networks and elucidate the mechanisms behind them.

In Sec. 1, we demonstrate that the linear and nonlinear peaks are two different phenomena by showing that they can co-exist in noisy regression tasks. This leads to a sample-wise *triple descent*, as sketched in Fig. 1. We consider both an analytically tractable model of random features [24] and a more realistic model of neural networks.

In Sec. 2, we provide a theoretical analysis of this phenomenon in the random feature model. Following [6, 19], we examine both the eigenspectrum of random feature Gram matrices and a bias-variance decomposition of the test loss. We show that the linear peak is solely caused by overfitting the noise corrupting the labels, whereas the nonlinear peak is also reinforced by the variance due to the initialization of the random feature vectors (which plays the role of the initialization of the weights in neural networks).

Finally, in Sec. 3, we present the phenomenological differences which follow from the theoretical analysis. Increasing the degree of nonlinearity of the activation function implicitly regularizes the

²The name “triple descent” refers to the presence of two peaks instead of just one in the famous “double descent” curve, but in most cases the test error does not actually descend before the first peak.

linear peak and strengthens the nonlinear peak. We also find that the nonlinear peak can be suppressed by regularizing or ensembling, whereas the linear peak cannot. Finally, we note that the linear peak appears much earlier under gradient descent dynamics than the nonlinear peak.

Related work Various sources of sample-wise non-monotonicity have recently been studied in different contexts. In the scenario of adversarial training, [25] shows that increasing N can help or hurt generalization depending on the strength of the adversary. In the non-parametric setting of [25], an upper bound on the test loss is shown to exhibit *multiple descent*, with peaks at each $N = D^i, i \in \mathbb{N}$.

Perhaps most related to our work, [18] observes a form of sample-wise triple descent in a non-isotropic linear regression task. In their setup, the two peaks stem from the covariance structure of the input data, which presents two eigenspaces of different strengths; both peaks boil down to what we would call “linear peaks” in this paper. The triple descent presented here is of different nature: it stems from the general properties of nonlinear projections, rather than the particular structure of the input data. To the best of our knowledge, the disentanglement of linear and nonlinear peaks presented here is novel.

Reproducibility We release the code necessary to reproduce the figures in this paper at <https://github.com/sdascoli/triple-descent-paper>.

1 Triple descent in the test loss phase space

We compute the (P, N) phase space of the test loss on noisy regression tasks to demonstrate the triple descent phenomenon. We start by introducing the two models which we will study throughout the paper: on the analytical side, the random feature model, and on the numerical side, a teacher-student task involving neural networks trained with gradient descent.

Dataset For both models, the input data $\mathbf{X} \in \mathbb{R}^{N \times D}$ consists of N vectors in D dimensions whose elements are drawn i.i.d. from $\mathcal{N}(0, 1)$. For each model, there is an associated label generator f^* corrupted by additive Gaussian noise: $y = f^*(\mathbf{x}) + \epsilon$, where the noise variance is inversely related to the signal to noise ratio (SNR), $\epsilon \sim \mathcal{N}(0, 1/\text{SNR})$.

1.1 Random features model

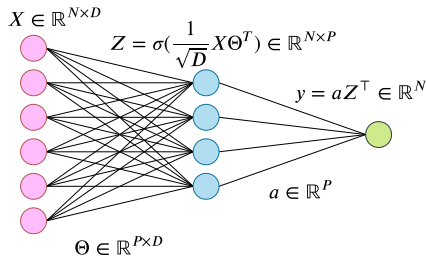


Figure 2: Illustration of an RF network.

Model We consider the random features (RF) model introduced in [24]. It can be viewed as a two-layer neural network whose first layer is a fixed random matrix $\Theta \in \mathbb{R}^{P \times D}$ (see Fig. 2)³:

$$f(\mathbf{x}) = \sum_{i=1}^P \mathbf{a}_i \sigma \left(\frac{\langle \Theta_i, \mathbf{x} \rangle}{\sqrt{D}} \right). \quad (1)$$

σ is a pointwise activation function, the choice of which will be of prime importance in the study. The ground truth is a linear model given by $f^*(\mathbf{x}) = \langle \beta, \mathbf{x} \rangle / \sqrt{D}$. Elements of Θ and β are drawn i.i.d from $\mathcal{N}(0, 1)$.

³This model, shown to undergo double descent in [12], has become a cornerstone to study the so-called lazy learning regime of neural networks where the weights stay close to their initial value [26]: assuming $f_{\theta_0} = 0$, we have $f_{\theta}(\mathbf{x}) \approx \nabla_{\theta} f_{\theta}(\mathbf{x})|_{\theta=\theta_0} \cdot (\theta - \theta_0)$ [27]. In other words, lazy learning amounts to a linear fitting problem with a random feature vector $\nabla_{\theta} f_{\theta}(\mathbf{x})|_{\theta=\theta_0}$.

Training The second layer weights, i.e. the elements of \mathbf{a} , are calculated via ridge regression with a regularization parameter γ :

$$\hat{\mathbf{a}} = \arg \min_{\mathbf{a} \in \mathbb{R}^P} \left[\frac{1}{N} (\mathbf{y} - \mathbf{aZ}^\top)^2 + \frac{P\gamma}{D} \|\mathbf{a}\|_2^2 \right] = \frac{1}{N} \mathbf{y}^\top \mathbf{Z} \left(\boldsymbol{\Sigma} + \frac{P\gamma}{D} \mathbb{I}_P \right)^{-1} \quad (2)$$

$$\mathbf{Z}_i^\mu = \sigma \left(\frac{\langle \boldsymbol{\Theta}_i, \mathbf{X}_\mu \rangle}{\sqrt{D}} \right) \in \mathbb{R}^{N \times P}, \quad \boldsymbol{\Sigma} = \frac{1}{N} \mathbf{Z}^\top \mathbf{Z} \in \mathbb{R}^{P \times P} \quad (3)$$

1.2 Neural networks

Model We consider a teacher-student neural network (NN) framework where a *student* network learns to reproduce the labels of a *teacher* network. The teacher f^* is taken to be an untrained ReLU fully-connected network with 2 layers and 100 nodes per layer. The student f is a fully-connected network with 2 layers and nonlinearity σ . Both are initialized with the default PyTorch initialization. Input dimension is set to $D=196$.

Training We train the student with mean-square loss using full-batch gradient descent for 1000 epochs with a learning rate of 0.01 and momentum 0.9⁴. We examine the effect of regularization by adding weight decay with parameter 0.05, and the effect of ensembling by averaging over 10 initialization seeds for the weights. All results are averaged over 10 runs.

1.3 Test loss phase space

In both models, the key quantity of interest is the *test loss*, defined as the mean-square loss evaluated on fresh samples $\mathbf{x} \sim \mathcal{N}(0, 1)$: $\mathcal{L}_g = \mathbb{E}_{\mathbf{x}} \left[(f(\mathbf{x}) - f^*(\mathbf{x}))^2 \right]$. In the case of the RF model, this quantity was derived rigorously in [12], and more recently in [28] by different approach which is used here compute the analytical phase space.

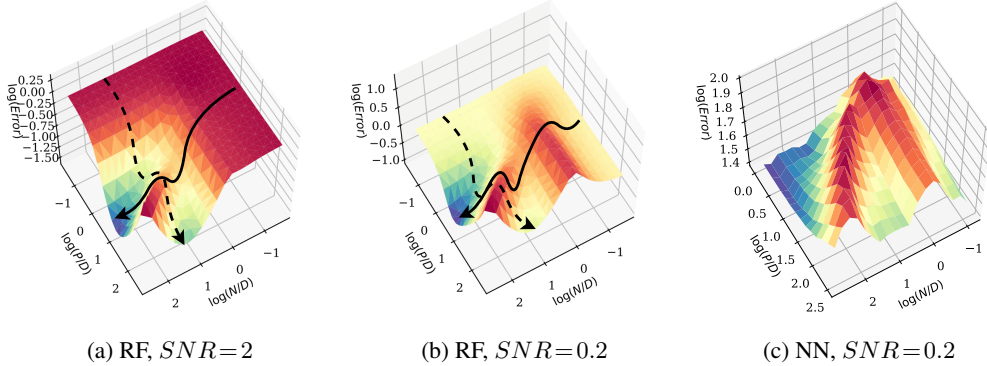


Figure 3: Logarithmic plot of the test loss in the (P, N) phase space. **(a)**: RF model with $\text{SNR} = 2$, $\gamma = 10^{-1}$. **(b)**: RF model with $\text{SNR} = 0.2$, $\gamma = 10^{-1}$. The solid arrows emphasize the sample-wise profile, and the dashed lines emphasize the parameter-wise profile. **(c)**: NN model. In all cases, $\sigma = \text{Tanh}$. Analogous results for different activation functions and values of the SNR are shown in Sec. A of the SM.

In Fig.3, we plot the test loss as a function of two intensive ratios of interest: the number of parameters per dimension P/D and the number of training examples per dimension N/D . In the left panel we show the usual parameter-wise and sample-wise double descent which occurs for the RF model at high SNR. However when the SNR becomes smaller than unity (middle panel), the sample-wise profile undergoes triple descent. This three-dimensional representation makes clear that the linear and nonlinear peaks are distinct. A qualitatively identical situation is shown for the NN model in the right panel⁵.

⁴We use full batch gradient descent with small learning rate to reduce the noise coming from the optimization as much as possible. After 1000 epochs, all observables appear to have converged.

⁵Note that for NNs, we necessarily have $P/D > 1$.

Structured data The case of structured datasets like MNIST is discussed in Sec. C of the SM. Although conclusions are very similar to the RF model, the NN model presents interesting differences which will be studied in future work.

2 Theory for the RF model

The qualitative similarity between the central and right panels of Fig. 3 indicates that a full understanding can be gained by a theoretical analysis of the RF model, which we present in this section by using methods developed recently for high-dimensional nonlinear models [12, 29] and RF Gram matrices [30, 31, 32, 33, 34].

2.1 High-dimensional setup

As is usual for the study of RF models, we consider the following high-dimensional limit:

$$N, D, P \rightarrow \infty, \quad \frac{D}{P} = \psi = \mathcal{O}(1), \quad \frac{D}{N} = \phi = \mathcal{O}(1) \quad (4)$$

Then the key quantities governing the behavior of the system are related to the properties of the nonlinearity around the origin:

$$\eta = \int dz \frac{e^{-z^2/2}}{\sqrt{2\pi}} \sigma^2(z), \quad \zeta = \left[\int dz \frac{e^{-z^2/2}}{\sqrt{2\pi}} \sigma'(z) \right]^2 \quad \text{and} \quad r = \frac{\zeta}{\eta} \quad (5)$$

As explained in [34], the Gaussian Equivalence Theorem [12, 29] which applies in this high dimensional setting establishes an equivalence to a *Gaussian covariate model* where the nonlinear activation function is replaced by a linear term and a nonlinear term acting as noise:

$$\mathbf{Z} = \sigma \left(\frac{\mathbf{X} \Theta^\top}{\sqrt{D}} \right) \rightarrow \sqrt{\zeta} \frac{\mathbf{X} \Theta^\top}{\sqrt{D}} + \sqrt{\eta - \zeta} \mathbf{W}, \quad \mathbf{W} \sim \mathcal{N}(0, 1) \quad (6)$$

Of prime importance is the degree of linearity $r = \zeta/\eta \in [0, 1]$, which indicates the relative magnitudes of the linear and the nonlinear terms⁶.

2.2 Spectral analysis

As expressed by Eq. 3, RF regression is equivalent to linear regression on a structured dataset $\mathbf{Z} \in \mathbb{R}^{N \times P}$, which is projected from the original i.i.d dataset $\mathbf{X} \in \mathbb{R}^{N \times D}$. In [6], it was shown that the peak which occurs in unregularized linear regression on i.i.d. data is linked to vanishingly small (but non-zero) eigenvalues in the covariance of the input data. Indeed, the norm of the interpolator needs to become very large to fit small eigenvalues according to Eq.3, yielding high variance.

Following this line, we examine the eigenspectrum of $\Sigma = \frac{1}{N} \mathbf{Z}^\top \mathbf{Z}$, which was derived in a series of recent papers. The spectral density $\rho(\lambda)$ can be obtained from the resolvent $G(z)$ [30, 31, 32, 33]:

$$\rho(\lambda) = \frac{1}{\pi} \lim_{\epsilon \rightarrow 0^+} \text{Im} G(\lambda - i\epsilon), \quad G(z) = \frac{\psi}{z} A \left(\frac{1}{z\psi} \right) + \frac{1 - \psi}{z}$$

$$A(t) = 1 + (\eta - \zeta) t A_\phi(t) A_\psi(t) + \frac{A_\phi(t) A_\psi(t) t \zeta}{1 - A_\phi(t) A_\psi(t) t \zeta} \quad (7)$$

where $A_\phi(t) = 1 + (A(t) - 1)\phi$ and $A_\psi(t) = 1 + (A(t) - 1)\psi$. We solve the implicit equation for $A(t)$ numerically, see for example Eq. 11 of [30].

In the bottom row of Fig. 4 (see also middle panel of Fig. 5), we show the numerical spectrum obtained for various values of N/D with $\sigma = \text{Tanh}$, and we superimpose the analytical prediction obtained from Eq. 7. At $N > D$, the spectrum separates into two components: one with D large

⁶Note from Eq. 5 that for non-homogeneous functions such as Tanh , r also depends on the variance of the inputs and fixed weights, both set to unity here: intuitively, smaller variance will yield smaller preactivations which will lie in the linear region of the Tanh , increasing the effective value of r .

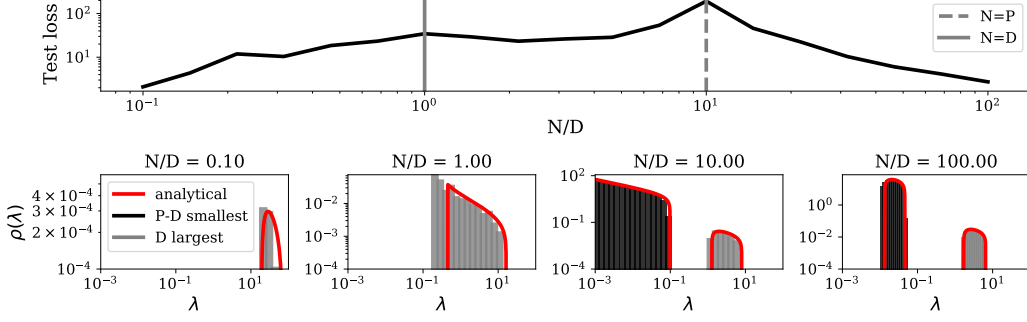


Figure 4: Eigenspectrum of the covariance of the projected features $\Sigma = \frac{1}{N} \mathbf{Z}^\top \mathbf{Z}$ at various values of N/D , with the corresponding test loss curve shown above. Analytics and numerics match well even at $D = 100$. We color the top D eigenvalues in gray, which allows to separate the linear and nonlinear components at $N > D$. We set $\sigma = \text{Tanh}$, $P/D = 10$, $\text{SNR} = 0.2$, $\gamma = 10^{-5}$.

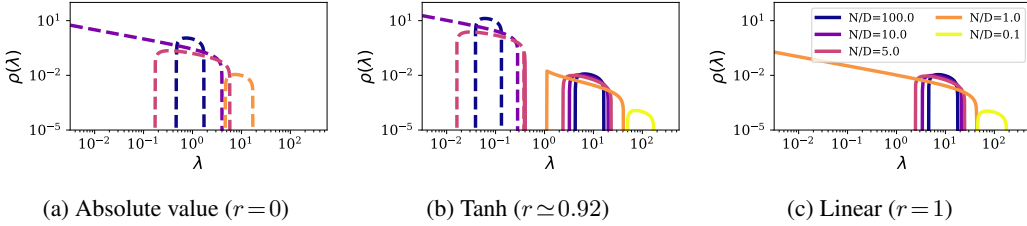


Figure 5: Eigenspectrum of Σ for $\eta = 1$, $P/D = 10$, and $\zeta = 0, 0.92, 1$ (a,b,c). We distinguish linear and nonlinear components by using respectively solid and dashed lines.

eigenvalues, and the other with $P - D$ smaller eigenvalues. The spectral gap (distance of the left edge of the spectrum to zero) closes at $N = P$, causing the nonlinear peak [35], but remains finite at $N = D$.

Fig. 5 shows the effect of varying r on the spectrum. We can interpret the results from Eq. 6:

- **Purely nonlinear** ($r = 0$): the spectrum of $\Sigma_{nl} = \frac{1}{N} \mathbf{W}^\top \mathbf{W}$ follows a Marcenko-Pastur distribution of parameter $c = P/N$, concentrating around $\lambda = 1$ at $N/D \rightarrow \infty$. The spectral gap closes at $N = P$.
- **Purely linear** ($r = 1$): the spectrum of $\Sigma_l = \frac{1}{ND} (\mathbf{X} \Theta^\top)^\top \mathbf{X} \Theta^\top$ follows a product Wishart distribution [36, 37], concentrating around $\lambda = P/D = 10$ at $N/D \rightarrow \infty$. The spectral gap closes at $N = D$.
- **Intermediate** ($r = 0.92$): we recognize the linear and nonlinear components, which behave almost independently (they are simply shifted to the left by a factor of r and $1 - r$ respectively), except at $N = D$ where they interact in an interesting way (see below).

Analysis of gaps For $r = 0$ the gap closes at $N = P$ whereas for $r = 1$ it closes at $N = D$. The former phenomenon still takes place for $0 < r < 1$, but the same cannot be said for the latter. The reason for this is that a vanishing gap is symptomatic of a random matrix reaching its maximal rank. Since $\text{rk}(\Sigma_{nl}) = \min(N, P)$ and $\text{rk}(\Sigma_l) = \min(N, P, D)$, we have $\text{rk}(\Sigma_{nl}) \geq \text{rk}(\Sigma_l)$ at $P > D$. Therefore, the rank of Σ is imposed by the nonlinear component, which only reaches its maximal rank at $N = P$. At $N = D$, the nonlinear component acts as an implicit regularization, by compensating the vanishing eigenvalues of the linear component.

Consequences on the peaks At $0 < r < 1$ and vanishing regularization, the norm of the estimator $\|\mathbf{a}\|$ diverges at $P = N$, yielding a diverging *nonlinear peak* in the test loss. No such divergence occurs at $N = D$ due to the implicit regularization, but a *linear peak* remains as a vestige of what happens at $r = 1$. A closer look at the spectrum clarifies the nature of this phenomenon. Notice in Fig. 5.b that although the lowest eigenvalue of the full spectrum is by no means minimal at $N = D$,

the left edge of the linear component reaches a minimum at $N = D$. This causes a peak in $\|\Theta \mathbf{a}\|$, the norm of the linearized network (see Sec. B of the SM for more details), which entails a different kind of overfitting as we explain below.

2.3 Bias-variance decomposition

The analysis of the eigenspectrum suggests that both peaks are related to some kind of overfitting. To address this issue, we make use of the bias-variance decomposition presented in [19]. The test loss is broken down into four contributions: a bias term and three variance terms stemming from the randomness of (i) the random feature vectors Θ (which plays the role of initialization variance in realistic networks), (ii) the noise ϵ corrupting the labels of the training set (noise variance) and (iii) the inputs \mathbf{X} (sampling variance). We defer to [19] for further details.

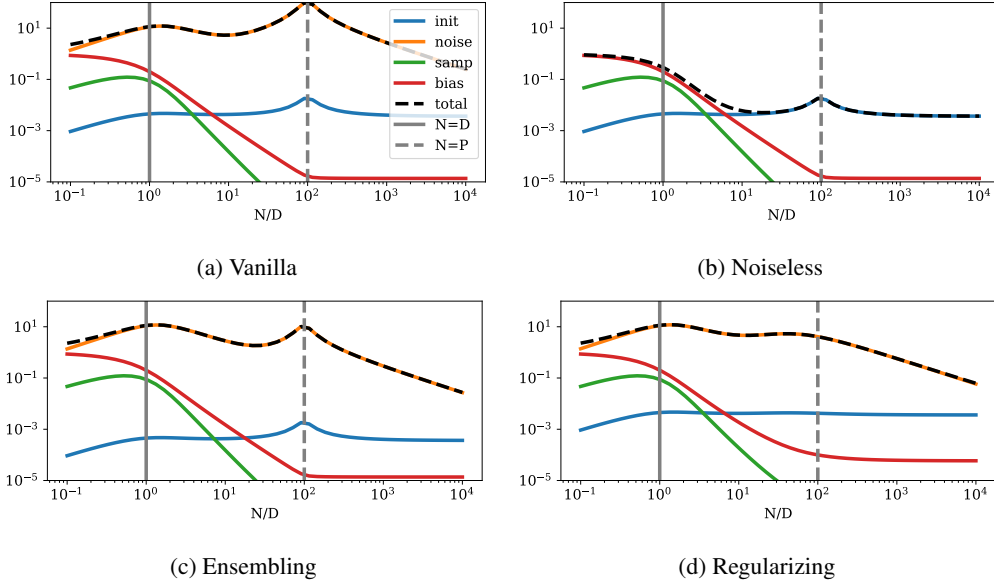


Figure 6: Bias-variance decomposition of the test loss in the RF model for $\sigma = \text{ReLU}$ and $P/D = 100$. Regularizing (increasing γ) and ensembling (increasing the number K of initialization seeds we average over) mitigates the nonlinear peak but does not affect the linear peak. **(a)** $K = 1, \gamma = 10^{-5}, SNR = 0.2$. **(b)** Same but $SNR = \infty$. **(c)** Same but $K = 10$. **(d)** Same but $\gamma = 10^{-3}$.

In Fig. 6, we show such a decomposition. As observed in [19], the nonlinear peak is caused by an interplay between initialization and noise variance. This peak appears starkly at $N = P$ in the high noise setup (upper left), where noise variance dominates the test loss, but also in the noiseless setup (upper right), where the residual initialization variance dominates. In contrast, the linear peak is caused solely by noise variance (upper left) in agreement with [6], and therefore vanishes in the noiseless setup (upper right). This is expected, as for linear networks the solution to the minimization problem is independent of the initialization of their weights.

3 Phenomenology of triple descent

3.1 Effect of the nonlinearity

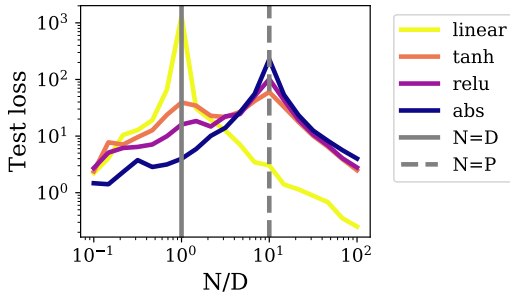


Figure 7: Numerical test loss of RF models at finite size ($D = 100$), averaged over 10 runs. We set $P/D = 10$, $SNR = 0.2$ and $\gamma = 10^{-3}$.

In Fig. 7, we consider four different activation functions: absolute value ($r = 0$), ReLU ($r = 0.5$), Tanh ($r \sim 0.92$) and linear ($r = 1$). We see that increasing the degree of linearity increases the strength of the linear peak and decreases the strength of the nonlinear peak, as expected from the theory above. In Sec. A of the SM, we present additional results where r is varied systematically in the RF model, and show that replacing Tanh by ReLU in the NN setup produces a similar effect. Note that the behavior changes abruptly near $r = 1$, marking the transition to the linear regime.

3.2 Effect of ensembling and regularization

It is a well-known fact that regularization [18] and ensembling [10, 19, 38] can mitigate the nonlinear peak. This is shown in the bottom row of Fig. 6 for the RF model. However, we see that these procedures only weakly affect the linear peak, which is already implicitly regularized for $r < 1$.

In the NN model, we perform a similar experiment by using weight decay as a proxy for the regularization procedure, see Fig. 8. Similarly as in the RF model, both ensembling and regularizing attenuates the nonlinear peak while leaving the linear peak almost untouched.

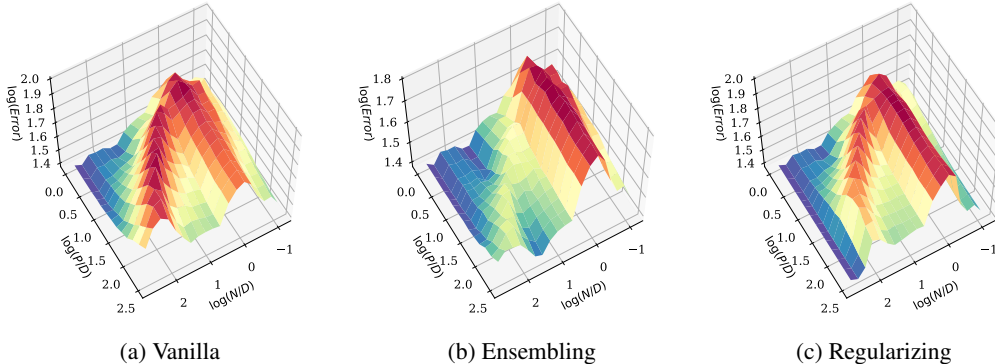


Figure 8: Test loss phase space for the NN model with $\sigma = \text{Tanh}$. Weight decay with parameter γ and ensembling over K seeds weakens the nonlinear peak but leaves the linear peak untouched. **(a)** $K = 1$, $\gamma = 0$, $SNR = 0.2$. **(b)** Same but $K = 10$. **(c)** Same but $\gamma = 0.05$.

3.3 Time dependence

To study the evolution of the phase space during training dynamics, we focus on the NN model (there are no dynamics involved in the RF model). In Fig. 9, we see that the linear peak appears early during training and maintains throughout, whereas the nonlinear peak only forms at late times. This can be understood qualitatively as follows [6]: for linear regression the time required to learn a mode of eigenvalue λ in the covariance matrix is proportional to λ^{-1} . Since the nonlinear peak is due to vanishingly small eigenvalues, which is not the case of the linear peak, the nonlinear peak takes more time to form completely.

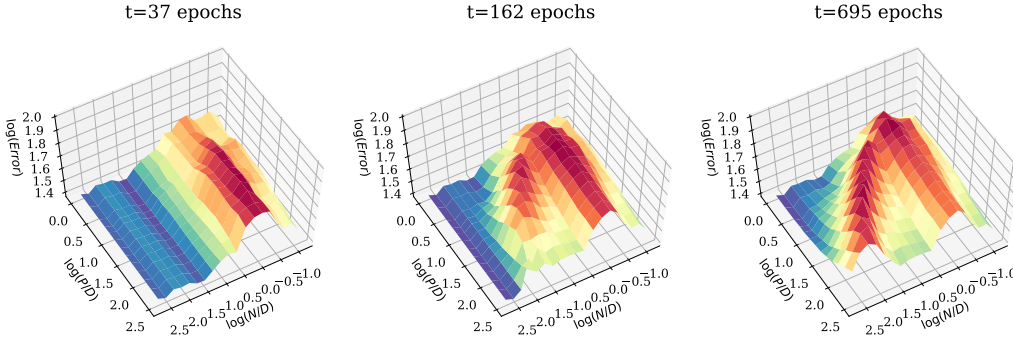


Figure 9: Test loss phase space for the NN model with $\sigma = \text{Tanh}$, plotted at various times during training. The linear peak grows first, followed by the nonlinear peak.

Conclusion

One of the key challenges in solving tasks with network-like architectures lies in choosing an appropriate number of parameters P given the properties of the training dataset, namely its size N and dimension D . By elucidating the structure of the (P, N) phase space, its dependency on D , and distinguishing the two different types of overfitting which it can exhibit, we believe our results can be of interest to practitioners.

Our results leave room for several interesting follow-up questions, among which the impact of (1) various architectural choices, (2) the optimization algorithm, and (3) the structure of the dataset. For future work, we will consider extensions along those lines with particular attention to the structure of the dataset. We believe it will provide a deeper insight into data-model matching.

Acknowledgements We thank Federica Gerace, Florent Krzakala, Bruno Loureiro, Franco Pellegrini, Maria Refinetti, Matthieu Wyart and Lenka Zdeborova for insightful discussions. GB acknowledges funding from the French government under management of Agence Nationale de la Recherche as part of the "Investissements d'avenir" program, reference ANR-19-P3IA-0001 (PRAIRIE 3IA Institute) and from the Simons Foundation collaboration Cracking the Glass Problem (No. 454935 to G. Biroli)

References

- [1] Alex Krizhevsky, Ilya Sutskever, and Geoffrey E Hinton. Imagenet classification with deep convolutional neural networks. In *Advances in neural information processing systems*, pages 1097–1105, 2012.
- [2] Yann LeCun, Yoshua Bengio, and Geoffrey Hinton. Deep learning. *nature*, 521(7553):436–444, 2015.
- [3] Geoffrey Hinton, Li Deng, Dong Yu, George E Dahl, Abdel-rahman Mohamed, Navdeep Jaitly, Andrew Senior, Vincent Vanhoucke, Patrick Nguyen, Tara N Sainath, et al. Deep neural networks for acoustic modeling in speech recognition: The shared views of four research groups. *IEEE Signal processing magazine*, 29(6):82–97, 2012.
- [4] Ilya Sutskever, Oriol Vinyals, and Quoc V Le. Sequence to sequence learning with neural networks. In *Advances in neural information processing systems*, pages 3104–3112, 2014.
- [5] Chiyuan Zhang, Samy Bengio, Moritz Hardt, Benjamin Recht, and Oriol Vinyals. Understanding deep learning requires rethinking generalization. *arXiv preprint arXiv:1611.03530*, 2016.
- [6] Madhu S Advani and Andrew M Saxe. High-dimensional dynamics of generalization error in neural networks. *arXiv preprint arXiv:1710.03667*, 2017.
- [7] Behnam Neyshabur, Zhiyuan Li, Srinadh Bhojanapalli, Yann LeCun, and Nathan Srebro. Towards understanding the role of over-parametrization in generalization of neural networks. *arXiv preprint arXiv:1805.12076*, 2018.

- [8] Mikhail Belkin, Daniel Hsu, Siyuan Ma, and Soumik Mandal. Reconciling modern machine learning and the bias-variance trade-off. *arXiv preprint arXiv:1812.11118*, 2018.
- [9] Brady Neal, Sarthak Mittal, Aristide Baratin, Vinayak Tantia, Matthew Scicluna, Simon Lacoste-Julien, and Ioannis Mitliagkas. A modern take on the bias-variance tradeoff in neural networks. *arXiv preprint arXiv:1810.08591*, 2018.
- [10] Mario Geiger, Arthur Jacot, Stefano Spigler, Franck Gabriel, Levent Sagun, Stéphane d’Ascoli, Giulio Biroli, Clément Hongler, and Matthieu Wyart. Scaling description of generalization with number of parameters in deep learning. *Journal of Statistical Mechanics: Theory and Experiment*, 2020(2):023401, 2020.
- [11] S Spigler, M Geiger, S d’Ascoli, L Sagun, G Biroli, and M Wyart. A jamming transition from under-to over-parametrization affects generalization in deep learning. *Journal of Physics A: Mathematical and Theoretical*, 52(47):474001, 2019.
- [12] Song Mei and Andrea Montanari. The generalization error of random features regression: Precise asymptotics and double descent curve. *arXiv preprint arXiv:1908.05355*, 2019.
- [13] Manfred Opper and Wolfgang Kinzel. Statistical mechanics of generalization. In *Models of neural networks III*, pages 151–209. Springer, 1996.
- [14] Andreas Engel and Christian Van den Broeck. *Statistical mechanics of learning*. Cambridge University Press, 2001.
- [15] Florent Krzakala and Jorge Kurchan. Landscape analysis of constraint satisfaction problems. *Physical Review E*, 76(2):021122, 2007.
- [16] Silvio Franz and Giorgio Parisi. The simplest model of jamming. *Journal of Physics A: Mathematical and Theoretical*, 49(14):145001, 2016.
- [17] Mario Geiger, Stefano Spigler, Stéphane d’Ascoli, Levent Sagun, Marco Baity-Jesi, Giulio Biroli, and Matthieu Wyart. Jamming transition as a paradigm to understand the loss landscape of deep neural networks. *Physical Review E*, 100(1):012115, 2019.
- [18] Preetum Nakkiran, Prayaag Venkat, Sham Kakade, and Tengyu Ma. Optimal regularization can mitigate double descent. *arXiv preprint arXiv:2003.01897*, 2020.
- [19] Stéphane d’Ascoli, Maria Refinetti, Giulio Biroli, and Florent Krzakala. Double trouble in double descent: Bias and variance (s) in the lazy regime. *arXiv preprint arXiv:2003.01054*, 2020.
- [20] Trevor Hastie, Andrea Montanari, Saharon Rosset, and Ryan J Tibshirani. Surprises in high-dimensional ridgeless least squares interpolation. *arXiv preprint arXiv:1903.08560*, 2019.
- [21] Melikasadat Emami, Mojtaba Sahraee-Ardakan, Parthe Pandit, Sundeep Rangan, and Alyson K Fletcher. Generalization error of generalized linear models in high dimensions. *arXiv preprint arXiv:2005.00180*, 2020.
- [22] Andrew M Saxe, James L McClelland, and Surya Ganguli. Exact solutions to the nonlinear dynamics of learning in deep linear neural networks. *arXiv preprint arXiv:1312.6120*, 2013.
- [23] Andrew K Lampinen and Surya Ganguli. An analytic theory of generalization dynamics and transfer learning in deep linear networks. *arXiv preprint arXiv:1809.10374*, 2018.
- [24] Ali Rahimi and Benjamin Recht. Random features for large-scale kernel machines. In *Advances in neural information processing systems*, pages 1177–1184, 2008.
- [25] Tengyuan Liang, Alexander Rakhlin, and Xiyu Zhai. On the risk of minimum-norm interpolants and restricted lower isometry of kernels. *arXiv preprint arXiv:1908.10292*, 2019.
- [26] Arthur Jacot, Franck Gabriel, and Clément Hongler. Neural tangent kernel: Convergence and generalization in neural networks. In *Advances in neural information processing systems*, pages 8571–8580, 2018.
- [27] Lénaïc Chizat, Edouard Oyallon, and Francis Bach. On lazy training in differentiable programming. In H. Wallach, H. Larochelle, A. Beygelzimer, F. d’Alché Buc, E. Fox, and R. Garnett, editors, *Advances in Neural Information Processing Systems 32*, pages 2933–2943. Curran Associates, Inc., 2019.
- [28] Federica Gerace, Bruno Loureiro, Florent Krzakala, Marc Mézard, and Lenka Zdeborová. Generalisation error in learning with random features and the hidden manifold model. *arXiv preprint arXiv:2002.09339*, 2020.

- [29] Sebastian Goldt, Marc Mézard, Florent Krzakala, and Lenka Zdeborová. Modelling the influence of data structure on learning in neural networks. *arXiv preprint arXiv:1909.11500*, 2019.
- [30] Jeffrey Pennington and Pratik Worah. Nonlinear random matrix theory for deep learning. In *Advances in Neural Information Processing Systems*, pages 2637–2646, 2017.
- [31] Lucas Benigni and Sandrine Péché. Eigenvalue distribution of nonlinear models of random matrices. *arXiv preprint arXiv:1904.03090*, 2019.
- [32] Ben Adlam, Jake Levinson, and Jeffrey Pennington. A random matrix perspective on mixtures of nonlinearities for deep learning. *arXiv preprint arXiv:1912.00827*, 2019.
- [33] Zhenyu Liao and Romain Couillet. On the spectrum of random features maps of high dimensional data. *arXiv preprint arXiv:1805.11916*, 2018.
- [34] S Péché et al. A note on the pennington-worah distribution. *Electronic Communications in Probability*, 24, 2019.
- [35] Madhu Advani, Subhaneil Lahiri, and Surya Ganguli. Statistical mechanics of complex neural systems and high dimensional data. *Journal of Statistical Mechanics: Theory and Experiment*, 2013(03):P03014, 2013.
- [36] Thomas Dupic and Isaac Pérez Castillo. Spectral density of products of wishart dilute random matrices. part i: the dense case. *arXiv preprint arXiv:1401.7802*, 2014.
- [37] Gernot Akemann, Jesper R Ipsen, and Mario Kieburg. Products of rectangular random matrices: singular values and progressive scattering. *Physical Review E*, 88(5):052118, 2013.
- [38] Andrew Gordon Wilson and Pavel Izmailov. Bayesian deep learning and a probabilistic perspective of generalization. *arXiv preprint arXiv:2002.08791*, 2020.
- [39] Chunyuan Li, Heerad Farkhoor, Rosanne Liu, and Jason Yosinski. Measuring the intrinsic dimension of objective landscapes. *arXiv preprint arXiv:1804.08838*, 2018.
- [40] Alessio Ansuini, Alessandro Laio, Jakob H Macke, and Davide Zoccolan. Intrinsic dimension of data representations in deep neural networks. In *Advances in Neural Information Processing Systems*, pages 6109–6119, 2019.
- [41] Stefano Spigler, Mario Geiger, and Matthieu Wyart. Asymptotic learning curves of kernel methods: empirical data vs teacher-student paradigm. *arXiv preprint arXiv:1905.10843*, 2019.

A Effect of signal-to-noise ratio and nonlinearity

A.1 RF model

In the RF model, varying r can easily be achieved analytically and yields interesting results, as shown in Fig. 10⁷.

In the top panel, we see that the parameter-wise profile exhibits double descent for all degrees of linearity r and signal-to-noise ratio SNR, except in the linear case $r = 1$ which is monotonously decreasing. Increasing the degree of nonlinearity (decreasing r) and the noise (decreasing the SNR) simply makes the nonlinear peak stronger.

In the bottom panel, we see that the sample-wise profile is more complex. In the linear case $r = 1$, only the linear peak appears (except in the noiseless case). In the nonlinear case $r < 1$, the nonlinear peak appears is always visible; as for the linear peak, it is regularized away, except in the strong noise regime SNR > 1 when the degree of nonlinearity is small ($r > 0.8$), where we observe the triple descent.

Notice that both in the parameter-wise and sample-wise profiles, the test loss profiles change smoothly with r , except near $r = 1$ where the behavior abruptly changes, particularly at low SNR.

⁷We focus here on the practically relevant setup $N/D \gg 1$. Note from the (P, N) phase-space that things can be more complex at $N/D \lesssim 1$.

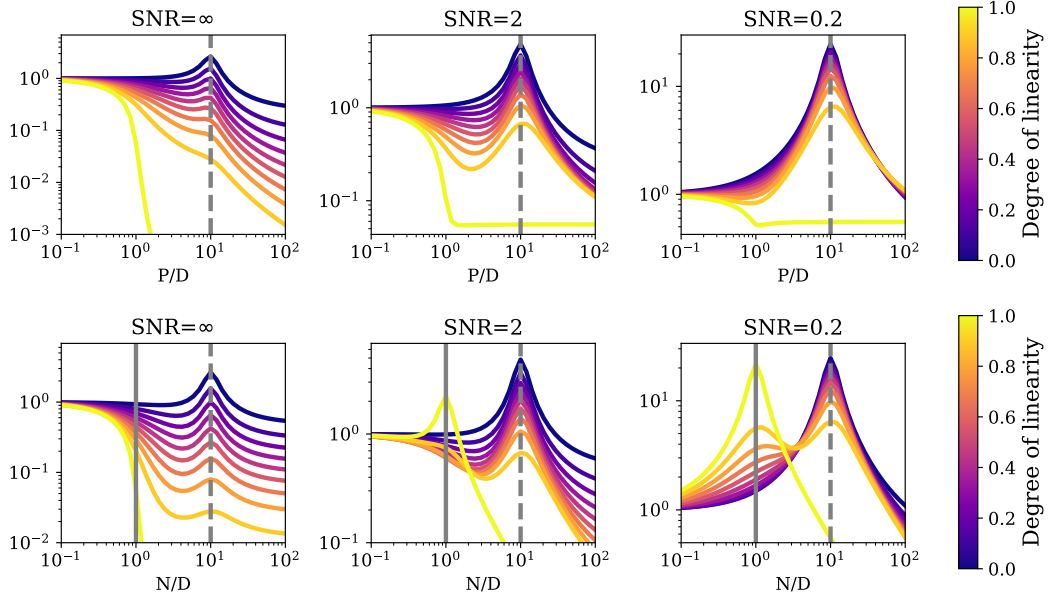


Figure 10: Analytical parameter-wise (**top**, $N/D = 10$) and sample-wise (**bottom**, $P/D = 10$) test loss profiles of the RF model. **Left**: noiseless case, $\text{SNR} = \infty$. **Center**: low noise, $\text{SNR} = 2$. **Right**: high noise, $\text{SNR} = 0.2$. We set $\gamma = 10^{-1}$.

One can also mimick these results numerically by considering, as in [30], the following family of piecewise linear functions:

$$\sigma_\alpha(x) = \frac{[x]_+ + \alpha[-x]_+ - \frac{1+\alpha}{\sqrt{2\pi}}}{\sqrt{\frac{1}{2}(1+\alpha^2) - \frac{1}{2\pi}(1+\alpha)^2}}, \quad (8)$$

for which

$$r_\alpha = \frac{(1-\alpha)^2}{2(1+\alpha^2) - \frac{2}{\pi}(1+\alpha)^2}. \quad (9)$$

Here, α parametrizes the ratio of the slope of the negative part to the positive part and allows to adjust the value of r continuously. $\alpha = -1$ ($r = 1$) will correspond to a (shifted) absolute value, $\alpha = 1$ ($r = 0$) will correspond to a linear function, $\alpha = 0$ will correspond to a (shifted) ReLU. In Fig. 11, we show the effect of sweeping α uniformly from 1 to -1 (which causes r to range from 0 to 1). As expected, we see the linear peak become stronger and the nonlinear peak become weaker.

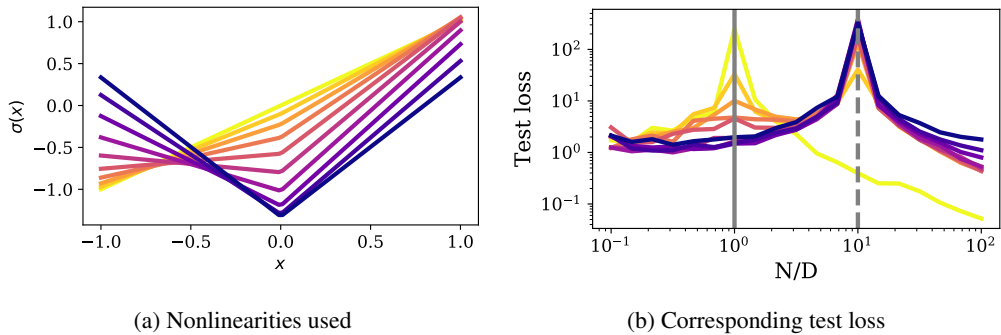


Figure 11: Moving from a purely nonlinear function to a purely linear function (dark to light colors) strengthens the linear peak and weakens the nonlinear peak.

A.2 NN model

We show in the top row of Fig. 12 the effect of varying the SNR on the (P, N) phase space for $\sigma = \text{Tanh}$ in the NN model. Just like in the RF model, triple descent only appears at $\text{SNR} < 1$ (right panel).

In the bottom row of the same figure, we show the effect of replacing Tanh ($r \sim 0.92$) by ReLU ($r = 0.5$). In the low SNR setup, we still distinguish the two peaks of triple descent, but the linear peak is much weaker, as expected from the stronger degree of nonlinearity.

Notice that in the intermediate signal-to-noise scenario, $1 < \text{SNR} < \infty$, results are different from the RF model where we only observed the nonlinear peak. For Tanh, we observe only the linear peak, whereas for ReLU, we observe something intermediate between the linear peak and the nonlinear peak.

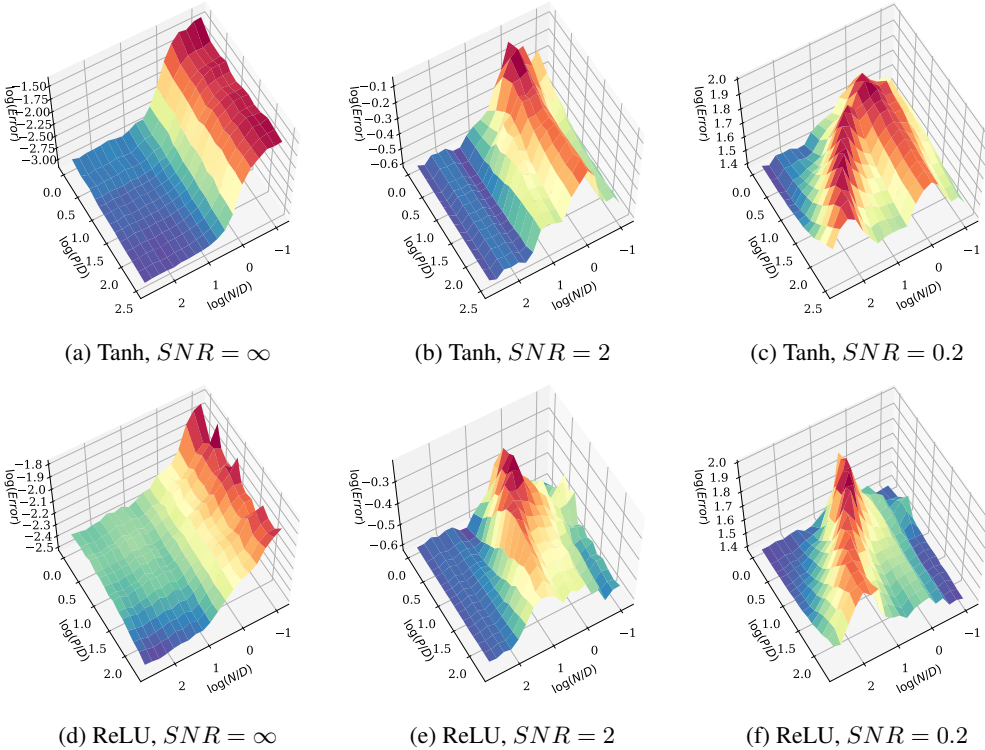


Figure 12: Logarithmic plot of the test loss in the phase space defined by number of parameters. **Left:** Single descent at low SNR. **Center:** Double descent at intermediate SNR. **Right:** Triple descent at low SNR.

B Origin of the linear peak

In this section, we follow the lines of [28], where the test loss is decomposed in the following way (Eq. D.6):

$$\mathcal{L}_g = \rho + Q - 2M \quad (10)$$

$$\rho = \frac{1}{D} \|\beta\|^2, \quad M = \frac{\sqrt{\zeta}}{D} \mathbf{b} \cdot \beta, \quad Q = \frac{\zeta}{D} \|\mathbf{b}\|^2 + \frac{\eta - \zeta}{P} \|\mathbf{a}\|^2, \quad \mathbf{b} = \Theta \mathbf{a} \quad (11)$$

As before, β denotes the linear teacher vector and Θ, \mathbf{a} respectively denote the (fixed) first and (learnt) second layer of the student. This insightful expression shows that the loss only depends on the norm of the second layer $\|\mathbf{a}\|$, the norm of the linearized network $\|\mathbf{b}\|$, and its overlap with the teacher $\mathbf{b} \cdot \beta$.

We plot these three terms in Fig. 13, focusing on the triple descent scenario $\text{SNR} < 1$. In the left panel, we see that the overlap of the student with the teacher is monotonically increasing, and reaches its maximal value at a certain point which increases from D to P as we decrease r from 1 to 0. In the central panel, we see that $\|\mathbf{a}\|$ peaks at $N = P$, causing the nonlinear peak as expected, but nothing special happens at $N = D$ (except for $r = 1$). However, in the right panel, we see that the norm of the linearized network peaks at $N = D$, where we know from the spectral analysis that the gap of the linear part of the spectrum is minimal. This is the origin of the linear peak.

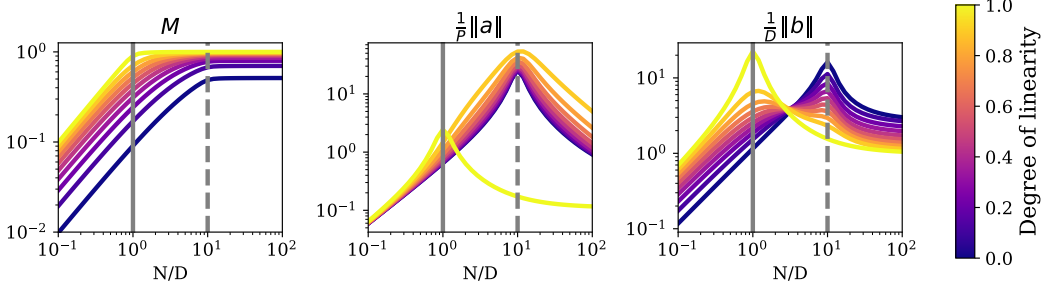


Figure 13: Terms entering Eq. 11, plotted at $\text{SNR} = 0.2$, $\gamma = 10^{-1}$.

C Structured datasets

In this section, we examine how our results are affected by considering the realistic case of correlated data. To do so, we replace the Gaussian i.i.d. data by MNIST data, downsampled to 10×10 images for the RF model ($D = 100$) and 14×14 images for the NN model ($D = 196$).

C.1 RF model

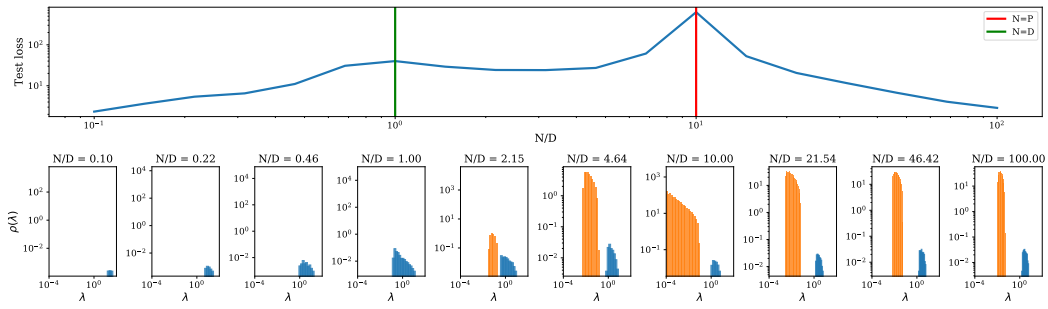
We refer to the results in Fig. 14. Interestingly, the triple descent profile is weakly affected by the correlated structure of this realistic dataset. However, the spectral properties of $\Sigma = \frac{1}{N}\mathbf{Z}^\top\mathbf{Z}$ are changed in an interesting manner: the two parts of the spectrum are now contiguous, there is no gap between the linear part and the nonlinear part.

C.2 NN model

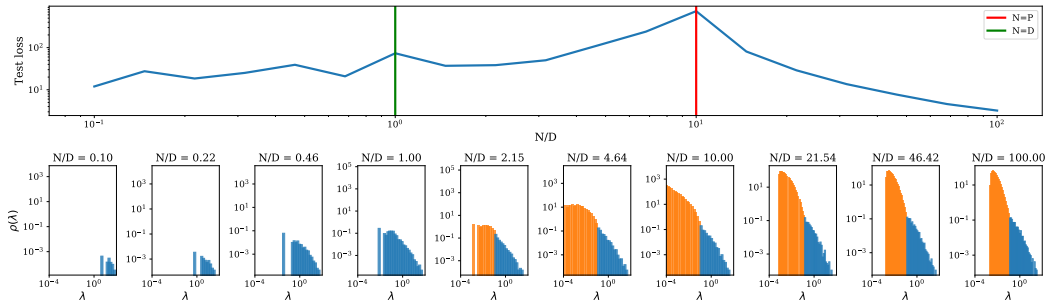
As shown in the top row of Fig. 15, the NN model is qualitatively different on the structured dataset: the two peaks at $N = D$ and $N = P$ are not well separated at $\text{SNR} < 1$ anymore. The single peak which appears is somewhat intermediate between the $N = D$ and $N = P$. However, by considering the time evolution in the bottom row of the same figure, we see that this peak shifts across the phase space during training, just like in the case of random data (Fig. 9).

At early times, it is located along a line of constant N , which makes it akin to a linear peak. At late times, it is rather reminiscent of a nonlinear peak, though it does not seem to be located at $P \sim N$ as before, but rather at $N \sim P^\alpha$ with $\alpha < 1$. This sublinear scaling is a consequence of the fact that structured data is easier to memorize than random data [17], and may blur the distinction between the two peaks.

Interestingly, at early times, the peak does not occur at $N = D$ as expected, but rather at $N = D_{\text{eff}} \sim D/10 \sim 20$. We hypothesize that D_{eff} may be related to the intrinsic dimension of the input data [39, 40, 41]. Although the linear peak still occurs at $N = D$ for MNIST data in the RF model, in the NN setup feature learning occurs. When the dataset is highly correlated like MNIST, feature learning compresses the dataset down to a more compact representation, likely causing the $N = D$ peak to shift to lower values. A study of this crucial question is deferred to future work.

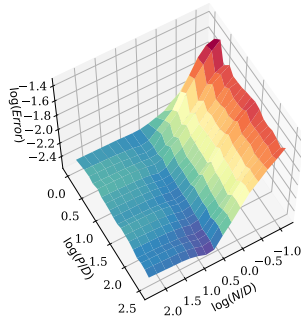


(a) Random data



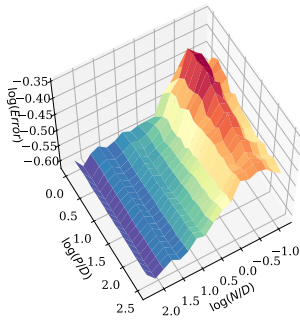
(b) MNIST

Figure 14: Spectrum of the covariance of the projected features $\Sigma = \frac{1}{N} \mathbf{Z}^\top \mathbf{Z}$ at various values of N/D , with the corresponding loss curve shown above. We set $\sigma = \text{Tanh}$, $\gamma = 10^{-5}$.



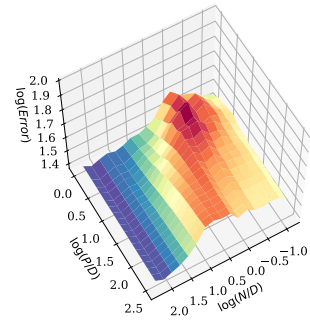
(a) MNIST, $SNR = \infty$

t=37 epochs



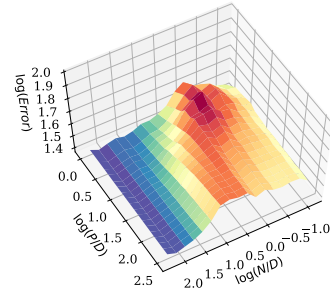
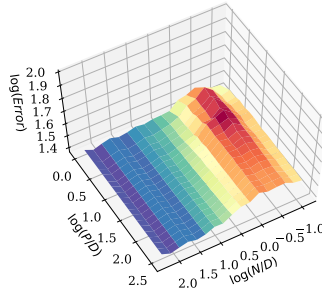
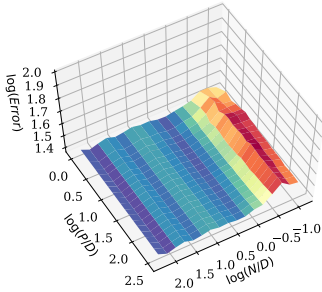
(b) MNIST, $SNR = 2$

t=162 epochs



(c) MNIST, $SNR = 0.2$

t=695 epochs



(d) Dynamics on MNIST at $SNR = 0.2$

Figure 15: Test loss phase space on MNIST with $\sigma = \text{ReLU}$. **Top:** After 1000 epochs, for various values of the SNR. **Bottom:** at three different times during training in the low SNR case.